Inorganic Chemistry

Article

pubs.acs.org/IC

Ratiometric Detection of Cr^{3+} and Hg^{2+} by a Naphthalimide-Rhodamine Based Fluorescent Probe

Prasenjit Mahato,[†] Sukdeb Saha,[†] E. Suresh,[†] Rosa Di Liddo,[‡] Pier Paolo Parnigotto,[‡] Maria Teresa Conconi,[‡] Manoj K. Kesharwani,[†] Bishwajit Ganguly,*[,†] and Amitava Das*[,†]

[†]Central Salt and Marine Chemicals Research Institute (CSIR), Bhavnagar -364002, Gujarat, India

[‡]Interdepartmental Research and Service Centre for Biology and Regenerative Medicine-Department of Pharmaceutical Sciences, University of Padua, Via Marzolo 5, 35131 Padua, Italy

Supporting Information

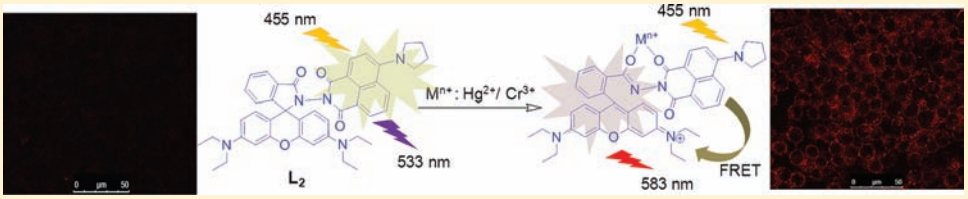

ABSTRACT: Newly synthesized rhodamine derivatives, $\mathbf{L_1}$ and $\mathbf{L_2}$, are found to bind specifically to Hg^{2+} or Cr^{3+} in presence of large excess of other competing ions with associated changes in their optical and fluorescence spectral behavior. These spectral changes are significant enough in the visible region of the spectrum and thus, allow the visual detection. For $\mathbf{L_1}$, the detection limit is even lower than the permissible $[Cr^{3+}]$ or $[Hg^{2+}]$ in drinking water as per standard U.S. EPA norms; while the receptor, **L2** could be used as a ratiometric sensor for detection of Cr^{3+} and Hg^{2+} based on the resonance energy transfer (RET) process involving the donor naphthalimide and the acceptor Cr^{3+}/Hg^{2+}-bound xanthene fragment. Studies reveal that these two reagents could be used for recognition and sensing of Hg^{2+}/Cr^{3+}. Further, confocal laser microscopic studies confirmed that the reagent $\mathbf{L_2}$ could also be used as an imaging probe for detection of uptake of these ions in A431 cells.

INTRODUCTION

Development of chemosensors for sensing and recognition of environmentally and biologically important heavy and transition metal ions, for example, Hg^{2+}, Pb^{2+}, Cu^{2+}, and Cr^{3+}, have attracted considerable attention of current researchers.[1,2] Among the heavy and transition metal ions, Hg^{2+} and Cr^{3+} appear ubiquitous because of various industrial and natural sources. Apart from that Hg^{2+} that is being released in the environment along with the effluent, atmospheric oxidation of mercury vapor also leads to the generation of water-soluble Hg^{2+} ions that deposit onto land or into water. Hg^{2+} is assimilated and converted by microorganisms to methylmercury, a potent neurotoxin.[3] Bioaccumulation of ionic mercury and methylmercury allows this toxin to get into the food chain.[4]

As an environmental contaminant, chromium is found mostly in Cr(VI) form and its bacterial reduction to Cr^{3+} is considered as one of the promising strategies for bioremediation.[5] However, a recent study reveals that soluble Cr^{3+} at pH 6−8 can be found transiently in significant concentrations and has a deleterious effect on microorganisms, like Shewanella sp. MR-4.[6] It is also proposed that Cr^{3+} ion, present in the cytoplasm, binds nonspecifically to DNA and other cellular components and inhibits transcription and possibly DNA replication.[7] Chromium deficiency is known to influence adversely the metabolism of glucose and lipids and cause maturity-onset diabetes, cardiovascular diseases, and nervous system disorders.[8] Thus, development of sensitive and selective chemosensors for Hg^{2+} and Cr^{3+} in various media is of considerable importance. In general, traditional analytical techniques like atomic absorption/emission spectroscopy or inductively coupled plasma mass spectrometry are costly and time-consuming methods, which are not convenient for "in-the-field" applications. Reports are there for electrochemical sensors for detection of these two ions.[9] However, among various methodologies that have been adopted for sensing of a specific analyte, fluorescence based sensors have been most popular for achieving higher sensitivity, rapid and reversible detection, and possible application in imaging studies for diagnostic applications.[10] Again Cr^{3+} is known to quench the luminescence of a fluorophore because of its paramagnetic property and Hg^{2+} quench due to effective spin−orbit coupling mechanism, bound to the receptor functionality of a sensor, and this accounts for the most fluorescence off/quenching-based sensors reported in the literature.[11] However, the preference is for the receptor with *fluorescence on* response because of the obvious ease in the detection process.

Among various photoinduced processes that are commonly involved in the signaling or response phenomena of luminescence based chemosensors, the resonance energy transfer (RET)[12] based process is preferred for designing an appropriate probe molecule over single dye-based probe

Received: September 23, 2011
Published: January 11, 2012

   dx.doi.org/10.1021/ic202073q | *Inorg. Chem.* 2012, 51, 1769−1777

molecules, as the RET based process is independent of the concentration of a single fluorescent dye and one can quantify the analyte concentration by using the ratio of intensities of the well resolved fluorescence peaks with reasonable intensities at two different wavelengths for analyte-free and analyte bound probe.[13] However, despite many advantages, examples of RET based *turn-on* fluorogenic sensors for Hg^{2+} and more specifically for Cr^{3+} in aqueous solution are not common in the literature.[14] Earlier reports on Cr^{3+} sensors, more than one metal ion (e.g., either Cu^{2+}, Zn^{2+}, Cd^{2+}[15] and Al^{3+} or Ni^{2+} and Cd^{2+}[16]) interfere with the detection processes. Keeping this in mind we have developed a new RET-based rhodamine derivative that is capable of reporting the Cr^{3+} binding process through a RET-based turn-on fluorescence response, while Hg^{2+} ion only interferes with the detection process. To understand the binding process and response phenomena well, we have also synthesized another naphthalimide derivative ($\mathbf{L_3}$) as a control. The change in spirocycle to open-ring form of the rhodamine fragment in $\mathbf{L_1}$ and $\mathbf{L_2}$ results in the remarkable enhancement of absorption or emission intensities, and these offer us the possibility of studying the Cr^{3+} or Hg^{2+} recognition process through the *switch-on* optical response—a criterion that is important for developing an in-field detection reagent.

EXPERIMENTAL SECTION

Rhodamine 6G, Rhodamine B, phthalic anhydride, 4-bromo-1,8-naphthalic anhydride, hydrazine hydrate, pyrrolidine, $Hg(ClO_4)_2$, $Cu(ClO_4)_2$, $Zn(ClO_4)_2$, $Ni(ClO_4)_2$, $Fe(ClO_4)_2$, $Pb(ClO_4)_2$, $Cd(ClO_4)_2$, $Cr(ClO_4)_3$, $Ca(ClO_4)_2$, $Co(ClO_4)_2$, $NaClO_4$, $KClO_4$, $Mg(ClO_4)_2$, $CsClO_4$, $Ba(ClO_4)_2$, $Sr(ClO_4)_2$, $AgClO_4$ were purchased from Sigma-Aldrich (U.S.A.). All the other reagents used were procured from S. D. fine chemicals, India. Acetonitrile, Methanol (AR; Merck, India), Ethanol (Spectrosol; Spectrochem, India) was used as a solvent. HPLC grade water (Merck, India) was used for experiments and spectral studies. ESI-MS measurements were carried out on Waters QTof-Micro instrument. Microanalysis (C, H, N) was performed using a Perkin-Elmer 4100 elemental analyzer. FTIR spectra were recorded as KBr pellets using a Perkin-Elmer Spectra GX 2000 spectrometer. ^{1}H and ^{13}C NMR spectra were recorded on Bruker 500 MHz FT NMR (model: Avance-DPX 500) and Bruker 200 MHz FT NMR (model: Avance-DPX 200). Electronic spectra were recorded with a Shimadzu UV-3101 PC/Varian Cary 500 Scan UV−vis−NIR Spectrophotometer. Fluorescence spectra recorded with a HORIBA JOBIN YVON spectrophotometer. Time resolved emission studies measurements were carried out with an Edinburgh OB920 spectrofluorimeter that works on Time Correlated Single Photon Counting (TCSPC) technique.

Synthetic Methodology. Rhodamine 6G hydrazide and Rhodamine B hydrazide were prepared following a literature method.[17]

Synthesis of $\mathbf{L_1}$. A 300 mg portion (0.7 mmol) of rhodamine-6G hydrazide was dissolved in 50 mL of dry acetonitrile by heating, with continuous stirring under N_2 atmosphere. Then 150 mg (0.77 mmol) of phthalic anhydride was added to the solution and then heated to reflux for 48 h. After that the reaction mixture was cooled to room temperature and evaporated to dryness. Then to the reaction mixture 30 mL of ethanol was added and stirred for about 3 h; a precipitate appeared which was filtered through G-4 crucible. The residue was washed several times with ethanol. Isolated yield of the compound $\mathbf{L_1}$ (yield was calculated based on the starting compounds) was 55% (215 mg, 0.38 mmol). ^{1}H NMR (500 MHz, DMSO-d_6, $Si(CH_3)_4$, J (Hz), δ (ppm)): 7.97 (1H, d, J = 7.5, H_j), 7.85 (4H, m, $H_{k,l,m,n}$), 7.75 (1H, t, H_i), 7.68 (1H, t, H_h), 7.21 (1H, d, J = 7.5, H_g), 6.35 (2H, s, H_f), 6.1 (2H, s, H_d), 5.07 (2H, s, H_c), 3.07−3.05 (4H, m, H_b), 1.91 (6H_e, s, H_e), 1.18 (6H, t, H_a). ^{13}C NMR (DMSO-d^6, 125 MHz, $Si(CH_3)_4$, δ (ppm)): 163.75, 163.54, 151.77, 150.98, 147.88, 135.59, 134.31, 129.82, 129.09, 128.74, 128.04, 124.55, 123.99, 123.06, 117.47, 103.4, 94.96, 66.74, 37.43, 17.15, 14.09. ESI-MS (*+ve* mode): m/z; 559.24 (100%) (M^++H^+), calc. for $C_{34}H_{30}N_4O_4$ is 558.6. Elemental Analysis data: Calc. C, 73.10; H, 5.41; N, 10.03; Expt. C, 73.3; H, 5.39; N, 9.96.

Synthesis of Intermediate Compound A. A 200 mg portion (0.44 mmol) of rhodamine B hydrazide and 121.5 mg of 4-bromo-1,8-naphthalic anhydride (0.44 mmol) were taken in 10 mL of glacial acetic acid to make a suspension. The suspension was heated to 110 °C for 24 h. Then it was cooled to room temperature and added to 40 mL of water. Then 1 M NaOH solution was added dropwise for neutralization to pH 8. A violet colored precipitate appeared which was filtered under vacuum in a G-3 crucible. Then the product was dried in vacuum desiccator. Isolated yield of the compound **A** (yield was calculated based on the starting compounds) was 95% (297 mg, 0.42 mmol). ^{1}H NMR (500 MHz, $CDCl_3$, $Si(CH_3)_4$, J (Hz), δ (ppm)): 8.53 (1H, d, J = 8.5, H_{11}), 8.3 (1H, d, J = 7, H_{12}), 8.07 (1H, d, J = 7, H_{14}), 8.03 (1H, d, J = 7.5, H_9), 7.94 (1H, d, J = 8, H_{10}), 7.76−7.67 (2H, m, $H_{7,8}$), 7.65 (1H, t, H_{13}), 7.31 (1H, d, J = 7.5, H_6), 6.68 (2H, d, J = 9, H_5), 6.38 (2H, d, J = 8, H_4), 6.07 (2H, br, H_3), 3.32−3.27 (8H, m, H_2), 1.09 (12H, t, H_1). ESI-MS (*+ve* mode): m/z; 717.77 (7%) (M^++H^+), calc. for $C_{40}H_{35}BrN_4O_4$ is 716.2. Elemental Analysis data: Calc. C, 67.13; H, 4.93; N, 7.83; Expt. C, 67.3; H, 4.97; N, 7.8.

Synthesis of $\mathbf{L_2}$. A 200 mg portion (0.28 mmol) of compound **A** was added to 10 mL of (excess) pyrrolidine and heated to reflux under inert atmosphere for 18 h with continuous stirring. The reaction mixture was cooled to room temperature and added to ice-cold water. A yellow colored precipitate appeared, which was filtered through a G-3 crucible. The product was washed several times with cold water and then dried under vacuum desiccator. Isolated yield of the compound $\mathbf{L_2}$ (yield was calculated based on the starting compounds) was 92% (181.5 mg, 0.26 mmol). ^{1}H NMR (500 MHz, CD_2Cl_2, $Si(CH_3)_4$, J (Hz), δ (ppm)): 8.54 (1H, d, J = 8.5, H_{28}), 8.17 (1H, d, J = 7.5, H_{24}), 8.05 (1H, d, J = 9, H_{26}), 8.01 (1H, d, J = 7.5, H_{23}) 7.69−7.61 (2H, m, $H_{21,22}$), 7.41 (1H, t, H_{27}), 7.26 (1H, d, J = 7.5, H_{25}), 6.71−6.69 (3H, m, J = 9, 2H_{19}, 1H_{20}), 6.37 (2H, d, J = 9, H_{18}), 6.11(2H, dd, J_1= 7.3, J_1= 2, H_{17}), 3.72 (4H, br, H_{29}), 3.32−3.29 (8H, m, H_{16}), 2.07−2.05 (4H, m, H_{30}), 1.1(12H, t, H_{15}) ^{13}C NMR (DMSO-d^6, 125 MHz, $Si(CH_3)_4$, δ (ppm)): 164.0, 161.6, 160.34, 154.34, 152.97, 148.78, 133.56, 131.06, 130.39, 129.55, 125.11, 123.55, 122.17, 121.57, 108.8, 108.23, 105.52, 97.34, 79.53, 67.41, 53.35, 44.22, 25.99, 12.7. ESI-MS (*+ve* mode): m/z; 706.09 (100%) (M^++H^+), calc. for $C_{44}H_{43}N_5O_4$ is 705.3. Elemental Analysis data: Calc. C, 74.87; H, 6.14; N, 9.92; Expt. C, 74.7; H, 6.2; N, 10.0.

Synthesis of the Intermediate B. A 750 mg portion (2.71 mmol) of 4-bromo naphthalic anhydride was added to 50 mL of ethanol and heated to reflux. To this suspension 132 μL (2.71 mmol) of hydrazine hydrate was added dropwise and heated to reflux for overnight; a yellow colored precipitate appeared. The reaction mixture was cooled to room temperature and filtered through G-4 crucible. The residue was washed several times with ethanol and then with slight ether. Isolated yield of the intermediate **B** (yield was calculated based on the starting compounds) was 91% (717 mg, 2.46 mmol). ^{1}H NMR (200 MHz, DMSO-d_6, $Si(CH_3)_4$, J (Hz), δ (ppm)): 8.55−8.47 (2H, m, $H_{33,35}$), 8.39 (1H, d, J = 7.8, H_{32}), 8.17 (1H, d, J = 7.8, H_{31}), 7.96 (1H, t, H_{34}), 5.78 (2H, s, H_{36}). ESI-MS (*+ve* mode): m/z; 315.1 (100%) (M^++Na^+), calc. for $C_{12}H_7BrN_2O_2$ is 292. Elemental Analysis data: Calc. C, 49.51; H, 2.42; N, 9.62; Expt. C, 49.3; H, 2.4; N, 9.7.

Synthesis of Intermediate C. Compound **C** was synthesized following a procedure similar to that for synthesis of $\mathbf{L_2}$ using the intermediate **B** instead of the intermediate **A**. Isolated yield of the intermediate **B** (yield was calculated based on the starting compounds) was 89% (430 mg, 1.6 mmol). ^{1}H NMR (200 MHz, DMSO-d_6, $Si(CH_3)_4$, J (Hz), δ (ppm)): 8.75 (1H, J = 8.4, d, H_{37}), 8.5 (1H, d, J = 7.2, H_{39}), 8.3 (1H, d, J = 8.8, H_{41}), 7.59 (1H, t, H_{38}), 6.87 (1H, d, J = 8.8, H_{40}) 3.83 (4H, t, H_{42}), 2.12 (4H, t, H_{43}). ESI-MS (*+ve* mode): m/z; 322.46 (100%) (M^++H_2O+Na^+), calc. for $C_{16}H_{15}N_3O_2$ is 281.31. Elemental Analysis data: Calc. C, 68.31; H, 5.37; N, 14.94; Expt. C, 68.1; H, 5.3; N, 14.9.

Synthesis of Compound $\mathbf{L_3}$. Compound $\mathbf{L_3}$ was synthesized by using the procedure as $\mathbf{L_1}$; while the intermediate **C** was used instead of rhodamine-6G hydrazide for the reaction. Isolated yield for $\mathbf{L_3}$ (yield was calculated based on the starting compounds) was 87.5%

dx.doi.org/10.1021/ic202073q | *Inorg. Chem.* 2012, 51, 1769−1777

Scheme 1. (a–c) Methodologies Adopted for the Synthesis of Necessary Intermediates (A, B, and C) and Final Receptor Molecules Like L_1, L_2, and L_3, and (d) X-ray Single Crystal Structure for L_1 and L_2

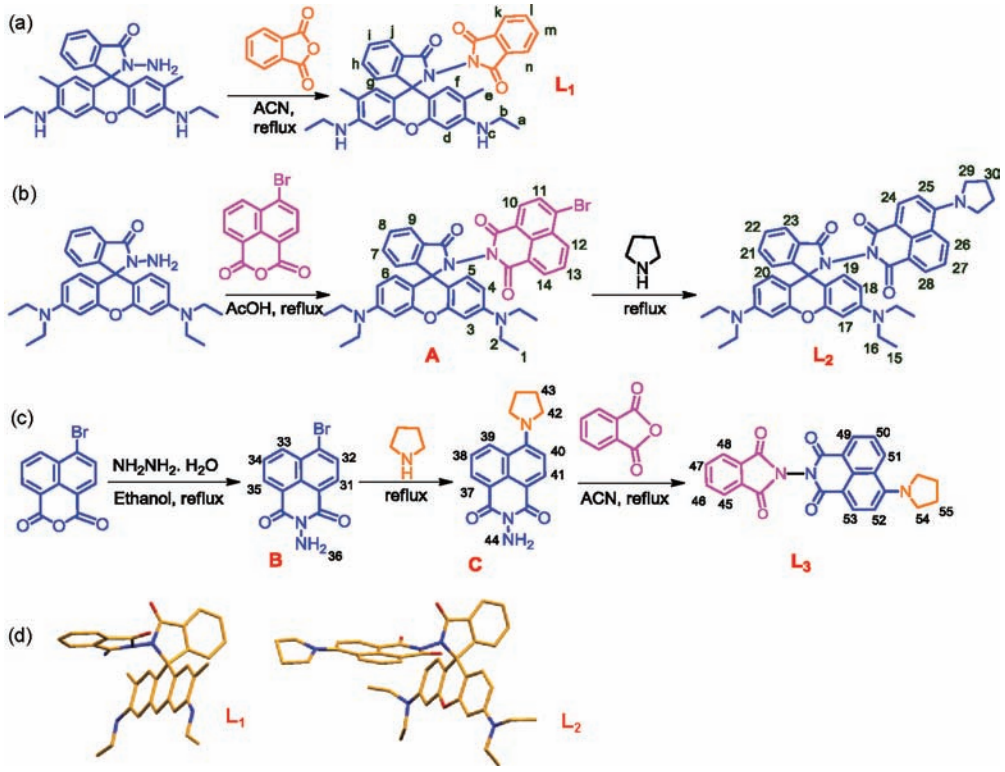

(512 mg, 1.24 mmol). ^{1}H NMR (200 MHz, DMSO-d_6, Si$(CH_3)_4$, J (Hz), δ (ppm)): 8.65 (1H, J = 8.6, d, H_{49}), 8.58 (1H, d, J = 7.2, H_{51}), 8.41(1H, d, J = 8.4, H_{53}), 7.97 (2H, d, J = 3.4, $H_{45,48}$), 7.83 (2H, d, J = 3.4, $H_{46,47}$), 7.55 (1H, t, H_{50}), 6.8 (1H, d, J = 8.8, H_{52}), 3.81 (4H, br, H_{54}), 2.12 (4H, br, H_{55}). ESI-MS (+*ve* mode): m/z; 434.4 (100%) (M^+ + Na^+) calc. for $C_{24}H_{17}N_3O_4$ = 411.4. Elemental Analysis data: Calc. C, 70.07; H, 4.16; N, 10.21; Expt. C, 70.3; H, 4.2; N, 10.2.

Biological Study. The efficacy of $\mathbf{L_2}$ as a sensor of Hg^{2+} and Cr^{3+} ions was studied in living human epidermoid A431 cells, as epithelia are the tissues mainly exposed to a risk of damage from an excess of Cr^{3+} and Hg^{2+}.[3a] The organic anion transporters are involved in the uptake of chromium[18] and mercury,[19] and they are nearly ubiquitously expressed in barrier epithelia.[19] Moreover, the overexpression of EGF receptors enhances the uptake of heavy metals upregulating the metal transporter proteins.[19] Sumalekshmy et al.[20] report that A431 cells present a rapid internalization of metal-ion indicators in living cells and are useful for in vitro testing. Confocal imaging experiments and flow cytometry were used to detect the emission of fluorescence in cells treated with $\mathbf{L_2}$ sensor after the exposure to Cr^{3+} or Hg^{2+}. In this work, A431 cells were obtained from EACC (Porton Down, Wilts, U.K.) and were cultured in Dulbecco's modified Eagle's medium (DMEM, Gibco, Carlsbad, CA), supplemented with 10% fetal bovine serum (FBS, Gibco) and 1% antibiotic solution (Gibco).

One day before testing, cells were trypsinized and seeded (5×10^3 cells/cm^2) on tissue culture plates (Falcon BD Biosciences, San José, CA) with glass or polystyrene surface for confocal and cytometrical analysis, respectively. The cells were incubated with 40 μM $Hg(NO_3)_2{\cdot}H_2O$ in DMEM or 50 μM $Cr(NO_3)_3{\cdot}9H_2O$ for 1 h at 37 °C, washed with PBS to remove the remaining mercury or chromium ions, and then incubated with 10 μM $\mathbf{L_2}$ in PBS for 30 min at 37 °C. In parallel, populations incubated only with $Hg(NO_3)_2{\cdot}H_2O$ or $Cr(NO_3)_3{\cdot}9H_2O$ solutions for 1 h or with only $\mathbf{L_2}$ solution for 30 min were prepared as controls. To have statistical significance, each sample was prepared in triplicate.

Confocal Microscopy. After treatment, all samples were kept in the incubator at 37 °C, 95% humidity, 0.5% CO_2 until the analysis. Confocal imaging experiments of living cells were performed in PBS, at room temperature, atmospheric atmosphere, for 5 min, and in dark. Data were acquired using a Leica TCS SP5 microscope (Leica Microsystems, Mannheim, Germany) with excitation light at 488 nm and filter cube N2.1 (bandpass 515–560 nm). As the activity of the $\mathbf{L_2}$ sensor was defined only by detecting an increased red fluorescence in samples with respect to the controls, the microscopic observation was performed without using any incubation and monitoring device suitable for a time-lapse study.

Cytometry. Treated samples and negative controls were washed twice with PBS and then mechanically reduced to a single cell suspension. All samples were kept in the incubator at 37 °C until analysis and then loaded on Moflo High speed cytometer (Beckman Coulter, Brea, CA, U.S.A.). The excitation of samples was performed at 488 argon laser, and the emission light was detected at 580 ± 30 nm. For the analysis, 2×10^4 cells were acquired by Summit 4.3 software, and results were expressed as mean fluorescence intensity (MFI) ± SD of samples with respect to controls. The statistical analysis was performed using *t-student* test.

Calculations for the Binding Constants Using Spectrophotometric Titration Data. The following equation was used for the nonlinear least-squares analysis[21] to determine the association constant, as well as the binding stoichiometry for the formation of the respective complex, $[Hg^{2+}{\cdot}\mathbf{L}]$ and $[Cr^{3+}{\cdot}\mathbf{L}]$ (where $\mathbf{L} = \mathbf{L_1}$ and $\mathbf{L_2}$),

$$A = (A_0 + A_{\lim}K_nC_M{}^n)/(1 + K_nC_M{}^n) \quad (1)$$

where A_0, A, and $A_{\lim}$ are the respective absorbance of free $\mathbf{L}$, $\mathbf{L}$ present in the form of $[Hg^{2+}{\cdot}\mathbf{L}]/[Cr^{3+}{\cdot}\mathbf{L}]$ in the complex, and $\mathbf{L}$ in presence of excess amounts of Hg^{2+} or Cr^{3+} ions where the absorbance reaches a limiting value. C_M is the metal ion concentration, K_n is the binding constant, and n is the stoichiometry of the complex formed between the ligand and metal ion.

Calculations for the Binding Constants Using Emission Titration Data. The following equation was used for the nonlinear least-squares analysis[21] to determine the association constant, as well as the binding stoichiometry for the formation of the respective complex, $[Hg^{2+}{\cdot}\mathbf{L}]$ and $[Cr^{3+}{\cdot}\mathbf{L}]$ (where $\mathbf{L} = \mathbf{L_1}$ and $\mathbf{L_2}$),

dx.doi.org/10.1021/ic202073q | *Inorg. Chem.* 2012, 51, 1769–1777

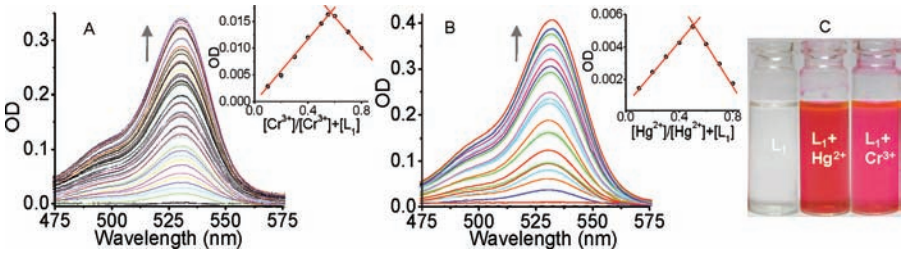

Figure 1. (A) Absorbance spectra of $\mathbf{L_1}$ (5 μM) with varying [Cr^{3+}] (0−1.34 mM) in CH_3CN-aq.HEPES buffer (1 mM, pH 7.2; 1:1, v/v). Inset: Jobs plot between $\mathbf{L_1}$ and Cr^{3+}. (B) Absorbance spectra of $\mathbf{L_1}$ (5.84 μM) with varying [Hg^{2+}] (0−0.51 mM) in CH_3CN-aq.HEPES buffer (1 mM, pH 7.2; 1:1, v/v). Inset: Jobs plot between $\mathbf{L_1}$ and Hg^{2+}. (C) Image of change of color of $\mathbf{L_1}$ in presence of 50 mol equivalent of Hg^{2+} and Cr^{3+}.

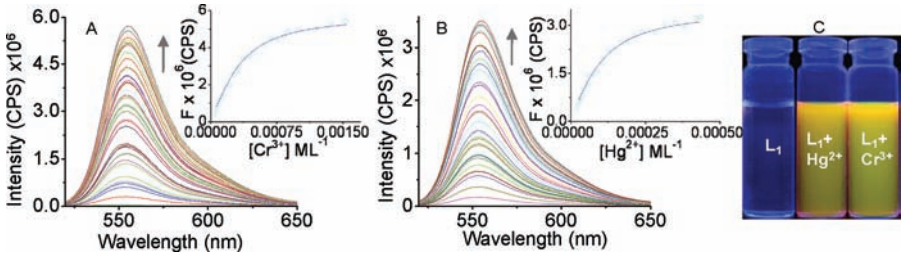

Figure 2. (A) Emission spectra of $\mathbf{L_1}$ (5 μM) with varying [Cr^{3+}] (0−1.34 mM) in CH_3CN-aq.HEPES buffer (1 mM, pH 7.2; 1:1, v/v). Inset: plot of emission intensity vs [Cr^{3+}]. (B) Emission spectra of $\mathbf{L_1}$ (5 μM) with varying [Hg^{2+}] (0−0.43 mM) in CH_3CN-aq.HEPES buffer (1 mM, pH 7.2; 1:1, v/v). Inset: plot of emission intensity vs [Hg^{2+}]. (c) Image of change of fluorescence of $\mathbf{L_1}$ in presence of 50 mol equiv of Hg^{2+} and Cr^{3+}.

$$F = (F_0 + F_{lim}K_n{C_M}^n)/(1 + K_n{C_M}^n) \quad (2)$$

where, F_0, F, and F_{lim} are the respective emission intensity of free **L**, **L** present in the form of $[Hg^{2+}\cdot\mathbf{L}]/[Cr^{3+}\cdot\mathbf{L}]$ in the complex, and **L** in presence of excess amounts of Hg^{2+} or Cr^{3+} ions where the emission intensity reaches a limiting value. C_M is the metal ion concentration, K_n is the binding constant, and n is the stoichiometry of the complex formed between the ligand and metal ion.

Evaluation of Different Parameters for FRET Process. The Förster distance R_0 was calculated using the expression shown in eq 3,

$$R_0 = 0.211[(J)Q(n^{-4})(\kappa^2)]^{1/6} \quad (3)$$

where, n is the refractive index of the medium in between donor and acceptor and was taken approximately to be equal to 1.4. κ^2 is the dipole orientation factor. Depending upon the relative orientation of donor and acceptor, the value ranges from 0−4, and it is often assumed to be 2/3. Q is the fluorescence quantum yield of the donor in the absence of acceptor. J is the spectral overlap integral between the emission spectrum of the donor and the absorption spectrum of the acceptor and is shown in the following eq 4,

$$J = \int f_D(\lambda)\, \varepsilon(\lambda)\lambda^4\, d\lambda \quad (4)$$

where $f_D(\lambda)$ is the normalized emission of the donor and $\varepsilon(\lambda)$ is the molar absorption coefficient (M^{-1} cm^{-1}) of the donor.

Energy transfer efficiency (Φ_{ET}) was evaluated using the expression shown in eq 5,

$$\Phi_{ET} = 1 - (F'_D/F_D) \quad (5)$$

where F'_D and F_D denote the donor fluorescence intensity with and without an acceptor, respectively.

Energy transfer rate constant (K_{ET}) was calculated using eq 6,

$$\Phi_{ET} = K_{ET}/(1/\tau_D + K_{ET}) \quad (6)$$

where τ_D denotes the fluorescence lifetime of the donor fragment in the absence of acceptor.

COMPUTATIONAL METHODS

All geometries for $\mathbf{L_1}$ and $Hg^{2+}\cdot\mathbf{L_1}$ were optimized by density functional theory (DFT) calculations using the Becke-3-Lee−Yang−Parr (B3LYP)[22] exchange functional and mixed basis set combinations that were given as general basis set input to Gaussian 09 (Gen keyword). The LANL2DZ basis sets were used for Hg^{2+}, whereas 6-31G* were used for other atoms.[23] All calculations were performed using Gaussian 09 program.[24]

RESULTS AND DISCUSSION

In the present study, we have carefully chosen rhodamine and 1,8-naphthalimide derivatives as the two fluorophores in synthesizing the receptor molecule $\mathbf{L_2}$; as absorption spectra of the Cr^{3+}/Hg^{2+} ion bound open spirocycle form of the rhodamine derivative develops a significant spectral overlap with the emission spectra of the *N*,*N*-dialkylamine-naphthalimide derivative and offers the possibility of a RET process. For free $\mathbf{L_2}$ FRET in its spirolactam form is otherwise suppressed, and only the yellow emission of the 1,8-naphthalimide derivative is observed upon excitation at 455 nm, the λ_{max} (absorption) for analogous derivative $\mathbf{L_3}$ (Scheme 1). Binding of $\mathbf{L_2}$ to Cr^{3+}/Hg^{2+} induces a RET process and results in an intense rhodamine-based red emission, which was confirmed by comparing results with analogous rhodamine derivative $\mathbf{L_1}$. Details about the synthesis of $\mathbf{L_1}$, $\mathbf{L_2}$, and $\mathbf{L_3}$ are discussed above and their characterization data are presented in the Supporting Information, Figures S1−S8. Proposed molecular structures of $\mathbf{L_1}$ and $\mathbf{L_2}$ were also confirmed by single crystal X-ray analysis (Scheme 1 and Supporting Information, Figures S9−S10).

UV−vis spectra recorded for $\mathbf{L_1}$ (CH_3CN-1.0 mM aq.HEPES buffer, pH = 7.2; 1:1, v/v) shows an absorption maximum at 300 nm, which was predominantly due to intraligand $\pi-\pi^*$ charge transfer (CT) transition. The binding ability of $\mathbf{L_1}$ was checked with perchlorate salts of Hg^{2+}, Cr^{3+}, Cu^{2+}, Pb^{2+}, Zn^{2+}, Co^{2+}, Ni^{2+}, Fe^{2+}, Ca^{2+}, Cd^{2+}, Mg^{2+}, K^+, Na^+, Sr^{2+}, Cs^+, Ba^{2+}, and Ag^+ in CH_3CN-aq.HEPES buffer (1 mM, pH 7.2; 1:1, v/v). A significant change in electronic spectral pattern was observed only with Hg^{2+} and Cr^{3+}, among all these metal ions used (Supporting Information, Figure S11). A new absorption band around 531 nm appeared with detectable change in solution

dx.doi.org/10.1021/ic202073q | Inorg. Chem. 2012, 51, 1769−1777

color from colorless to bright pink (Figure 1). The binding affinity for these two respective metal ions towards $\mathbf{L_1}$ was evaluated from spectrophotometric titration ($K_{Hg^{2+}}$ = 3.13 ± 0.08 × 10^5 M^{-1} and $K_{Cr^{3+}}$ = 1.38 ± 0.04 × 10^5 M^{-1} at 25 °C); while 1:1 binding stoichiometry was evaluated using nonlinear regression analysis (Figure 1, Supporting Information, Figure S12).[21] Subsequently, an intense emission band appeared at λ_{ems}^{max} = 557 nm on excitation at λ_{ext} = 500 nm, which was earlier absent for pure $\mathbf{L_1}$ (Figure 2). Thus a switch-on luminescence response was observed at 557 nm for $Cr^{3+}$and Hg^{2+}; while analogous experiment with other cations did not show any such enhancement (Supporting Information, Figure S11). Switch on responses for the absorption spectral band at 531 nm and the luminescence band at ~557 nm on binding to Hg^{2+} or Cr^{3+} suggest opening of the spirolactam ring in $\mathbf{L_1}$ on metal ion coordination. Association constant values, calculated from emission titration (Figure 2), for binding of $\mathbf{L_1}$ with Hg^{2+} and Cr^{3+} were found to be 3.07 ± 0.3 × 10^5 M^{-1} ($K_{Hg^{2+}}$) and 1.28 ± 0.08 × 10^5 M^{-1} ($K_{Cr^{3+}}$), respectively. These values are very close to the respective binding constant for Hg^{2+} and Cr^{3+}, obtained from electronic spectral titrations. Further, spectral studies revealed that a lower detection limit for Hg^{2+} and Cr^{3+} were 0.35 and 0.14 ppb (Supporting Information, Figures S13–S14) (for signal-to-noise ratio of 3:1), respectively, where the U.S. EPA limit for Hg^{2+} and Cr^{3+} (Cr^{3+} and Cr^{6+}) are 2 and 100 ppb respectively.[25]

Further $\mathbf{L_1}$ could be used as selective chemosensor for Cr^{3+}, while experiments were performed in presence of excess KI. On addition of the aqueous solution of KI to the pink colored solution of Hg^{2+}·$\mathbf{L_1}$, spectral bands (absorption band with λ_{Max} at 532 nm and emission band with λ_{Max} at ~557 nm for λ_{Ext} = 500 nm), as well as the color of the solution disappeared (Figure 3). Again on addition of Cr^{3+} to this solution mixture

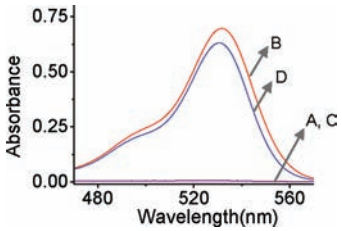

Figure 3. Absorption spectra of (A) $\mathbf{L_1}$ (17.9 μM), (B) $\mathbf{L_1}$ in presence of Hg^{2+} (0.2 mM), (C) $\mathbf{L_1}$ in presence of Hg^{2+} (0.2 mM) and KI (0.5 mM), (D) $\mathbf{L_1}$ in presence of Hg^{2+} (0.2 mM), KI (0.5 mM) and Cr^{3+} (0.36 mM) in CH_3CN-aq.HEPES buffer (0.01 M, pH 7.2; 1:1, v/v).

having KI, absorbance band at 530 nm and emission band at 557 nm reappeared (Figure 3, Supporting Information, Figure S15). Simultaneously, the pink color of the solution was also restored. Preferential binding of the iodide ion to the Hg^{2+} ion led to the formation of HgI_2 and the regeneration of the cyclic lactam form of the reagent, a process which is well documented for demonstrating the reversible binding of rhodamine derivatives to Hg^{2+}.[10m] However, the absorption and emission spectral bands, as well the solution color, were restored on coordination of the Cr^{3+} to $\mathbf{L_1}$. Further experiments reveal that the absorbance spectra for Cr^{3+}·$\mathbf{L_1}$ and its solution color remained unchanged on addition of excess of iodide ion in the form of KI (Supporting Information, Figure S16). Thus, in presence of excess of KI, reagent $\mathbf{L_1}$ could be used for selective recognition of Cr^{3+} from all other metal ions.

A binding stoichiometry of 1:1 was confirmed from the Job's plot for binding of Hg^{2+} or Cr^{3+} to $\mathbf{L_1}$ (inset of Figure 1). This 1:1 stoichiometry was further confirmed from results the ESI-MS studies (Supporting Information, Figure S17). FTIR spectra of $\mathbf{L_1}$ revealed that the peak at 1724 cm^{-1}, the characteristic stretching frequency for the CO_{Amide} bond of the rhodamine unit, shifted to 1610 cm^{-1} and 1611 cm^{-1} on coordination to the Hg^{2+} and Cr^{3+} ions, respectively, in presence of 1.5 equiv of the respective metal ion (Supporting Information, Figure S18). Such shift in the stretching frequency of CO_{Amide} bond of the rhodamine unit on binding to a metal ion is reported earlier.[26] Simultaneously, the stretching frequency band at 1744 cm^{-1}, corresponding to the carbonyl group of the phthalimide moiety, was shifted to 1646 and 1641 cm^{-1} in presence of 1.5 equiv of Hg^{2+} and Cr^{3+} ions, respectively. These appreciable shifts support the coordination of the $O_{>CO}$ of the rhodamine and phthalimide units to the Hg^{2+} or Cr^{3+} center and the possible binding mode for $\mathbf{L_1}$ to Hg^{2+} or Cr^{3+} ion is shown in Scheme 2. The generation of the

Scheme 2. Schematic Presentation Showing the Possible Metal Ion Binding Mode of $\mathbf{L_1}$

acyclic rhodamine form of $\mathbf{L_1}$, as shown in Scheme 2, was also confirmed by the electronic and fluorescence spectral studies (vide supra). However, the most convincing proof in favor of the ring-opening of the spirolactam form of $\mathbf{L_1}$ on coordination to Hg^{2+} ion was established from ^{13}C NMR studies. Results of the ^{13}C NMR studies revealed that the signal at 66.74 ppm for tertiary carbon of the spirolactam ring of $\mathbf{L_1}$ disappeared upon addition of Hg^{2+} (Supporting Information, Figure S19).

Spectral studies using a freshly prepared solution of compound $\mathbf{L_3}$ in identical mixed solvent medium (CH_3CN-1.0 mM aq.HEPES buffer, pH 7.2; 1:1, v/v) revealed that the emission spectra for $\mathbf{L_3}$ (*N*,*N*-dialkylamine-naphthalimide derivative) had a significant overlap with absorption spectra of rhodamine B (Figure 4),[14f] and this led us to develop a new

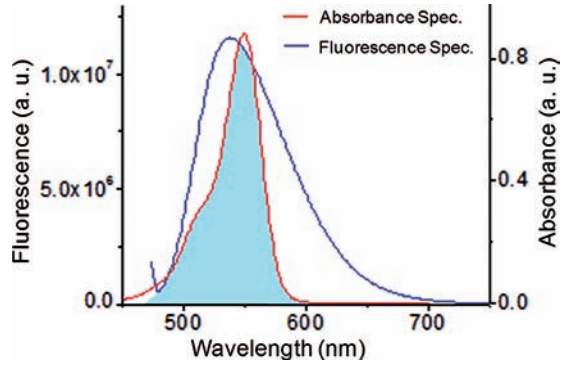

Figure 4. Overlap (shown with cyan shade) between emission and absorption spectra of the donor and acceptor, respectively.

receptor, $\mathbf{L_2}$ with an aim for developing a reagent for ratiometric sensing of Hg^{2+}/Cr^{3+}.

dx.doi.org/10.1021/ic202073q | Inorg. Chem. 2012, 51, 1769–1777

The spectral properties of L_2 in CH_3CN-1.0 mM aq.HEPES buffer (1 mM, pH 7.2; 1:1, v/v) were recorded. L_2 displayed absorption bands at 455 nm and on excitation at this wavelength a yellow fluorescence centered at 533 nm was observed; while L_3 showed an absorption band at 462 nm (Supporting Information, Figure S20). Thus, the absorption spectrum for L_2 was found to be the linear combination of spectra for L_1 and L_3 with little blue shift for the L_3-based absorption band (Supporting Information, Figure S20). Thus the emission at 533 nm, following excitation at 455 nm, is attributed to an intramolecular charge transfer (ICT) process associated with 1,8-naphthalimide chromophore;[27] while the rhodamine moiety retains its spirolactam form. In presence of Cr^{3+}/Hg^{2+}, the *switch on* response at 561 nm for electronic spectra and at 583 nm for luminescence spectra accounts for a visually detectable change in solution color and luminescence because of the opening of the spirolactam ring and generation of the delocalized xanthene moiety.[10h] It will not be unreasonable to presume that the similar binding motif for $Hg^{2+}\cdot L_2$ or $Cr^{3+}\cdot L_2$ formation, as it was proposed for the other reagent L_1 with analogous structure, would prevail for the reagent L_2. Results of the different spectral studies support this presumption. FTIR studies revealed that the characteristic stretching frequency for the CO_{Amide} of the rhodamine moiety at 1693 cm^{-1} was shifted to 1588 and 1589 cm^{-1} in presence of 1.5 equiv of Hg^{2+} and Cr^{3+}, respectively. Whereas the stretching frequency band at 1729 cm^{-1} for the $CO_{Naphthalimide}$ was shifted to 1644 and 1643 cm^{-1} in presence of 1.5 equiv of Hg^{2+} and Cr^{3+} (Supporting Information, Figure S18), respectively. Significant shifts in the stretching frequencies of both CO groups of naphthalimide and rhodamine moieties of L_2 support the proposed binding mode similar to that of L_1. The coordination site of L_2 for chelation with Hg^{2+} was also confirmed by ^1H NMR and ^{13}C NMR spectra (Figure 5 and Supporting Information, Figure S21). Disappearance of ^{13}C NMR signal at 66.85 ppm for tertiary carbon of the spirolactam ring of L_2 upon addition of Hg^{2+} confirmed the opening of the spirolactam ring and coordination through $O_{>CO}$ of the rhodamine moiety (Supporting Information, Figure S21). Chelation of Hg^{2+} through two $O_{>CO}$ atoms of L_2, as discussed above, is expected to deplete the electron density in the aromatic rings of the xanthene and 1,8-naphthalimide moieties, and this was reflected in the appreciable downfield shifts of the associated aromatic protons (Figure 5). These shifts were more pronounced for H_{17}, H_{18}, and H_{19} protons ($\Delta\delta$ = 1.1, 0.8, and 0.6 ppm, respectively), which revealed opening of the spirolactam ring on coordination to Hg^{2+} with associated charge transfer in the aromatic rings of the xanthene moiety. Downfield shift of H_{25}, H_{26}, H_{27}, and H_{28} ($\Delta\delta$ = 0.13, 0.05, 0.12, and 0.11 ppm, respectively) of the naphthalimide moiety indicates the involvement of its carbonyl oxygen in Hg^{2+} binding.

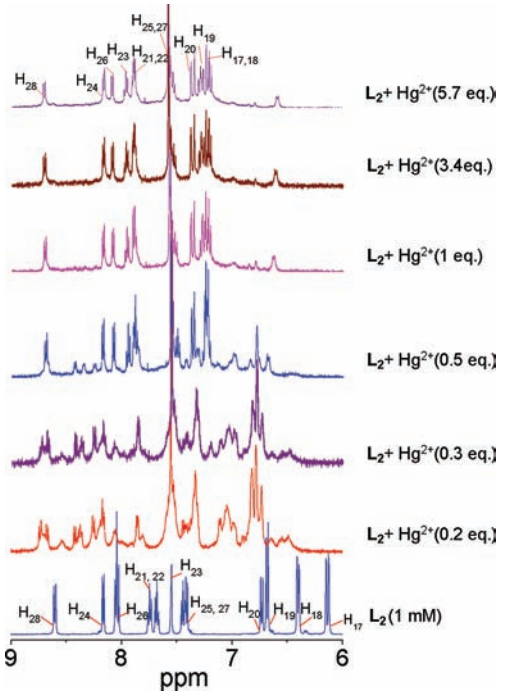

Figure 5. Partial ^1H NMR spectra for L_2 (1 mM) in presence of varying $[Hg^{2+}]$ (0–0.0057 M) in $CDCl_3$:CD_3OD = 1:1(v/v).

Spectral (Electronic and emission) responses for L_2 toward Hg^{2+} and Cr^{3+} in presence of excess of KI were similar as it was observed for L_1 (Supporting Information, Figure S22), which confirmed that this reagent also could be used for delineating Cr^{3+} from Hg^{2+} in mixed solvent medium (CH_3CN-1.0 mM aq.HEPES buffer,1:1 v/v) pH 7.2).

The binding of Cr^{3+}/Hg^{2+} ion induces opening of the spirolactam ring in L_2 with an associated switch on UV–vis spectral response in the range 515–585 nm, which has a significant spectral overlap with the emission spectrum of the *N,N*-dialkylamine-naphthalimide fragment and makes non-radiative transfer of excitation energy between donor naphthalimide to acceptor xanthene moiety feasible and initiates an intramolecular FRET process. Thus, with increasing $[Cr^{3+}]$ or $[Hg^{2+}]$, the $[Cr^{3+}\cdot L_2]$ or $[Hg^{2+}\cdot L_2]$ increases with associated increase in the absorbance intensity at 561 nm (Figure 6) and emission at 583 nm (for λ_{Ext} = 561 nm). Respective binding constant values for two metal ions ($K_{Cr^{3+}}$ = (1.22 ± 0.07) × 10^5 and $K_{Hg^{2+}}$ = (1.01 ± 0.05) × 10^5 M^{-1} at 25 °C) were evaluated from the absorbance titration using λ_{Mon} = 560 nm. Binding stoichiometry for the respective complex was evaluated using nonlinear regression analysis and was found to be for 1:1 for both cases.[21] On excitation at 455 nm, a steady decrease in emission intensity at 533 nm (characteristic for the naphthalimide moiety) was observed along with a concomitant increase in the intensity of the new fluorescence band at 583 nm (characteristic for spirocycle opening moiety) (Figure 7). A well-defined iso-emissive point appeared at 548 nm.

This also resulted in a visually detectable change in solution fluorescence (Figure 7). The binding constant values for two metal ions ($K_{Cr^{3+}}$ = (1.12 ± 0.01) × 10^5 and $K_{Hg^{2+}}$ = (1.09 ± 0.02) × 10^5 M^{-1} at 25 °C) were evaluated from the emission titrations using λ_{Mon} = 583 nm, and these values are comparable with those obtained from absorption titrations. The ratio of emission intensities for rhodamine moiety to 1,8-naphthalimide fragment at 583 and 533 nm (I_{583}/I_{533}), respectively, varied from 0.47 to 11.72, which correspond to a 25.1 fold enhancement in emission intensity in presence of Hg^{2+}; while this ratio for Cr^{3+} varied from 0.47 to 10.67 and resulted a 22.75 fold enhancement (Figure 7 and Supporting Information, Figure S23) in emission intensity.

For both metal ions, 1:1 complex formation was established from Job's plot and thus, corroborated our earlier observations on electronic spectral titration, as well from ESI-MS spectra (Supporting Information, Figure S24–S25). The noninterfering absorption bands with significant wavelength shift and the

dx.doi.org/10.1021/ic202073q | *Inorg. Chem.* 2012, 51, 1769–1777

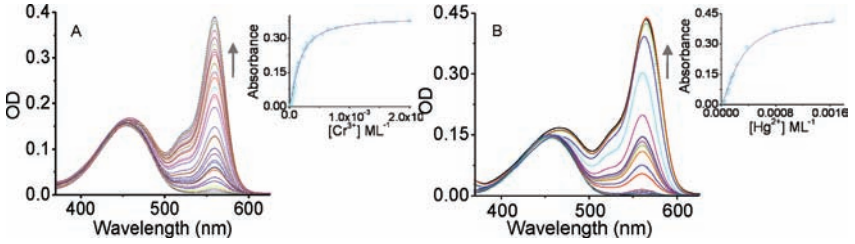

Figure 6. Electronic spectra of (A) $\mathbf{L}_2$ (6.7 μM) with varying [Cr^{3+}] (0−2.5 mM), inset: least square plot of absorbance vs [Cr^{3+}]; (B) of $\mathbf{L}_2$ (6.7 μM) with varying [Hg^{2+}] (0−3.2 mM), inset: least square plot of absorbance vs [Hg^{2+}]. All studies were carried out in CH_3CN-aq.HEPES buffer (1 mM, pH 7.2; 1:1, v/v) medium.

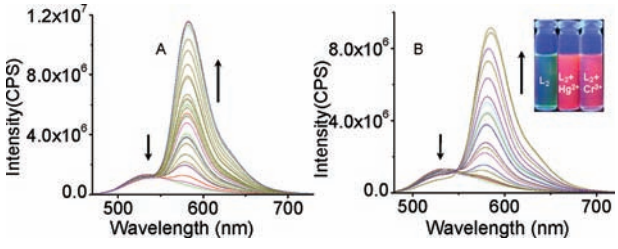

Figure 7. Fluorescence spectra of (A) $\mathbf{L}_2$ (6.96 μM) with varying [Cr^{3+}] (0−0.92 mM), and (B) of $\mathbf{L}_2$ (7.4 μM) with varying [Hg^{2+}] (0−0.1 mM), inset: image of change of fluorescence of $\mathbf{L}_2$ in presence of 50 mol equiv of Hg^{2+} and Cr^{3+}. All studies were carried out in CH_3CN-aq.HEPES buffer (1 mM, pH 7.2; 1:1, v/v) medium.

possibility to probe the binding of Cr^{3+}/Hg^{2+} in mixed aqueous organic medium at two emission maxima make the receptor $\mathbf{L}_2$ a unique ratiometric probe.

The singlet−singlet excitation energy-transfer efficiency (Φ_{ET}) and rate constant for the energy-transfer process (k_{ET}) between donor and acceptor were evaluated from steady state and time-resolved fluorescence data. The value for Φ_{ET} and k_{ET} was found to be 50% and 2.33×10^8 s^{-1}, respectively; while the Förster critical distance (R_0) was calculated as 64.5 Å.

Competitive binding of $\mathbf{L}_1$ and $\mathbf{L}_2$ to Cr^{3+}/Hg^{2+} were established in presence of 10 mol equiv of other metal ions like Cu^{2+}, Pb^{2+}, Zn^{2+}, Co^{2+}, Ni^{2+}, Fe^{2+}, Ca^{2+}, Cd^{2+}, Mg^{2+}, K^+, Na^+, Sr^{2+}, Cs^+, Ba^{2+}, and Ag^+ is discussed in Supporting Information (Supporting Information, Figure S26). Reversible binding of Cr^{3+}/Hg^{2+} to $\mathbf{L}_1$ and $\mathbf{L}_2$ was also established through spectral studies in presence of 3 mol equiv of Na_2EDTA (Supporting Information, Figure S27).

The proposed binding mode of the reagent $\mathbf{L}_1$ to Hg^{2+} was also investigated with density functional theory (DFT) calculations. All geometries were fully optimized using the B3LYP method and general basis set (Gen keyword).[22] The carbon, nitrogen, oxygen, and hydrogen atoms were calculated with 6-31G* basis set,[23] whereas Hg^{2+} was calculated with the LANL2DZ basis set. The B3LYP optimized geometry of $\mathbf{L}_1$ is similar to the structure obtained from crystal study (Scheme 1d and Figure 8). Since ESI-Mass spectra has suggested the coordination of two water molecules to Hg^{2+} complexed with $\mathbf{L}_1$ (Supporting Information, Figure S17), therefore, calculations have been performed with two coordinated water molecules. The optimized geometry suggests a distorted tetrahedral geometry around the Hg^{2+} ion (Figure 8). Studies revealed that $[Hg^{2+}\cdot\mathbf{L}_1]_{Spirolactam}$ is 277.3 kcal/mol more stable than separated reactants ($\mathbf{L}_1$ + $2H_2O$ + Hg^{2+}). In this complexed structure, Hg^{2+} binds with the spirolactam and phthalimide carbonyl oxygens of $\mathbf{L}_1$. The additional calculation was performed for optimizing the geometry for the $Hg^{2+}\cdot\mathbf{L}_1$ having the xanthene moiety. The calculated complex $Hg^{2+}\cdot\mathbf{L}_1$ was found to be more stable by 19.3 kcal/mol than that of $[Hg^{2+}\cdot\mathbf{L}_1]_{Spirolactam}$. Further, optimized structure for $Hg^{2+}\cdot\mathbf{L}_1$ reveals that Hg^{2+}-O_{II} distance (2.175 Å) is shorter than the Hg^{2+}-O_I distance (2.331 Å). This signifies a stronger binding through the CO_{II} of the xanthene moiety than the CO_I moiety of the phthalimide fragment. Thus, the calculated results corroborate the proposed binding mode (Scheme 2) for $Hg^{2+}\cdot\mathbf{L}_1$, and it will be reasonable to presume that similar binding mode will prevail for reagent $\mathbf{L}_2$.

Owing to its favorable properties, $\mathbf{L}_2$ sensor should be suited for fluorescence imaging in living cells. We evaluated the applicability of $\mathbf{L}_2$ as a probe of Hg^{2+} and Cr^{3+} by confocal

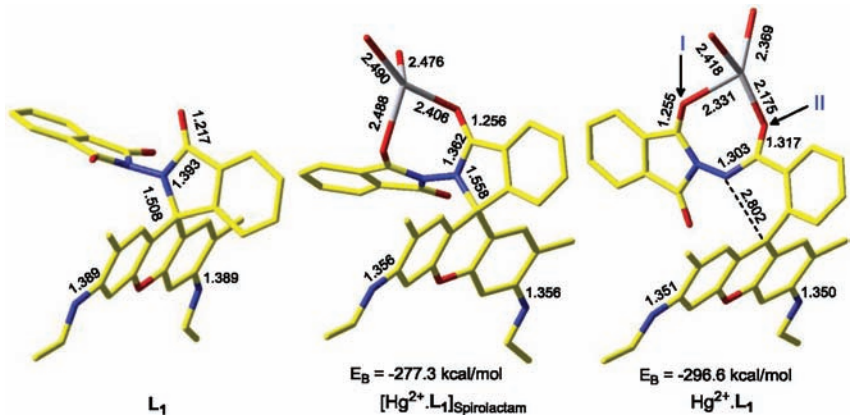

Figure 8. B3LYP optimized geometries and important bond distances (Å) of rhodamine derivative $\mathbf{L}_1$ and its complexes with Hg^{2+} ion. Binding energy (E_B) of complexes is also given. For clarity hydrogens are omitted (yellow = C; red = O; blue = N; light gray = Hg).

dx.doi.org/10.1021/ic202073q | Inorg. Chem. 2012, 51, 1769−1777

microscope (Leica TCS SP5) and cytometer (Moflo High Speed cytometer) on A431 cells treated with 50 μM $Cr(NO_3)_3$ or 40 μM $Hg(NO_3)_2$ for 1 h at 37 °C, and then with 10 μM $\mathbf{L_2}$ solution for 30 min at 37 °C.

As shown in Figure 9, a significant fluorescence emission from the intracellular region was observed (Figure 9 B, C), suggesting a subcellular distribution of Cr^{3+} and Hg^{2+} in the cytoplasm. In contrast, when the cells were treated with only 10 μM $\mathbf{L_2}$, 50 μM $Cr(NO_3)_3$ or 40 μM $Hg(NO_3)_2$ a negligible

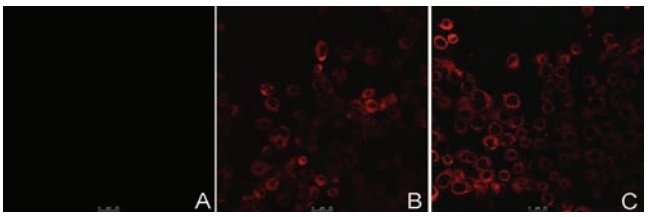

Figure 9. Confocal microscopic images of A431 cells (A) loaded with 10 μM $\mathbf{L_2}$, (B) 50 μM Cr^{3+} and 10 μM $\mathbf{L_2}$, (C) 40 μM Hg^{2+} and 10 μM $\mathbf{L_2}$.

intracellular fluorescence was detected (Figure 9A). The above results indicated that $\mathbf{L_2}$ was cell permeable and the marked enhancement of the intracellular red fluorescence confirmed the binding of $\mathbf{L_2}$ with Cr^{3+} and Hg^{2+} within A431 cells (Figure 9). Consistent with morphological studies, the cytometrical analysis by a Moflo High speed cytometer (Beckman Coulter) (Figure 10) detected a significant increase of fluorescent cells induced by $\mathbf{L_2}$ in samples treated respectively with Cr^{3+} (88.57% ± 1.45) (B) and Hg^{2+} (88.70% ± 0.30) (C) or versus $\mathbf{L_2}$ control (A). Performing the excitation with 488 argon

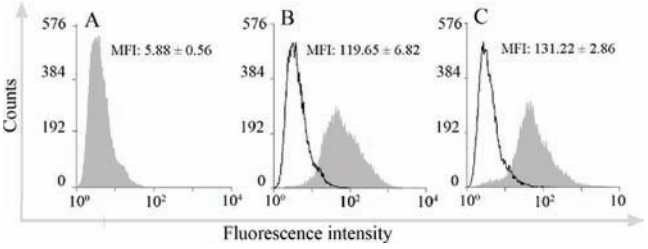

Figure 10. Cytometrical detection of $Cr^{3+}\cdot\mathbf{L_2}$ (B) and $Hg^{2+}\cdot\mathbf{L_2}$ (C) in A431 cells treated for 30 min with $\mathbf{L_2}$. Data are expressed as MFI ± SD of positive cells (gray peak) versus $\mathbf{L_2}$ control (black peak) (A).

laser and the emission detection at 580 ± 30 nm, the measured mean fluorescence intensity (MFI) rising from $Cr^{3+}\cdot\mathbf{L_2}$ and $Hg^{2+}\cdot\mathbf{L_2}$ was appreciably higher than that of $\mathbf{L_2}$ control.

In summary, we have developed sensitive and selective receptors ($\mathbf{L_1}$ and $\mathbf{L_2}$) for Cr^{3+} and Hg^{2+}, where binding to these two ions induces a turn on response in electronic and fluorescence spectra in the visible region. Thus, these receptors could be used as a dual probe for visual detection through change in color and fluorescence. In presence of excess KI, these two reagents bind specifically to Cr^{3+} and thus could discriminate these ions present as a mixture in aqueous solution. For $\mathbf{L_1}$, the detection limit is even lower than the permissible Cr^{3+}/Hg^{2+} concentration in drinking water as per standard norms; while the receptor $\mathbf{L_2}$ could be used as a ratiometric sensor for detection of Cr^{3+} and Hg^{2+} based on the RET process involving the donor naphthalimide and the acceptor Cr^{3+}/Hg^{2+}-bound xanthene fragment of $M^{n+}\cdot\mathbf{L_2}$. Model compounds $\mathbf{L_1}$ and $\mathbf{L_3}$ were synthesized to confirm the binding mode and the unambiguous assignment of the response processes. Probe molecule, like $\mathbf{L_2}$, which works in physiological conditions is preferred for use either as a colorimetric staining agent or as a reagent for imaging studies with biological and environmental samples. Moreover, when used on epithelial cells like A431, the reagent $\mathbf{L_2}$ could detect successfully the cellular uptake of Cr^{3+} or Hg^{2+} ion.

■ ASSOCIATED CONTENT

Ⓢ Supporting Information

Characterization, spectroscopic data and X-ray crystallographic data in CIF format of $\mathbf{L_1}$ (CCDC 829120) and $\mathbf{L_2}$ (CCDC 829121). Cartesian coordinates of all optimized geometries. This material is available free of charge via the Internet at http://pubs.acs.org.

■ AUTHOR INFORMATION

Corresponding Author

*Phone: +91 278 2567760 [672] (A.D.). Fax: +91 278 2656762 (A.D.). E-mail: amitava@csmcri.org (A.D.).

■ ACKNOWLEDGMENTS

A.D. acknowledges DST and CSIR for financial support. P.M. and S.S. acknowledge CSIR, and M.K.K. acknowledge UGC for research fellowship. R.D.L., P.P.P., and M.T.C. thank Saint Luca Hospital-ULSS 18 placed in Trecenta (Rovigo)-Italy for providing laboratory facilities.

■ REFERENCES

(1) (a) Desvergne, J. P.; Czarnik, A. W. *Chemosensors of Ion and Molecule Recognition*; Kluwer: Dordrecht, The Netherlands, 1997. (b) Spichiger-Keller, U. S. *Chemical Sensors and Biosensors for Medical and Biological Applications*; Wiley-VCH: Weinheim, Germany, 1998.

(2) (a) Jiang, P. G.; Chen, L. Z.; Lin, J.; Liu, Q.; Ding, J.; Gao, X.; Guo, Z. J. *Chem. Commun.* **2002**, 1424. (b) Zhang, H.; Han, L.-F.; Zachariasse, K. A.; Jiang, Y. B. *Org. Lett.* **2005**, *7*, 4217. (c) He, Q.; Miller, E. W.; Wong, A. P.; Chang, C. J. *J. Am. Chem. Soc.* **2006**, *128*, 9316. (d) Martinez, R.; Zapata, F.; Caballero, A.; Espinosa, A.; Tairraga, A.; Molina, P. *Org. Lett.* **2006**, *8*, 3235.

(3) (a) U.S. EPA, Regulatory Impact Analysis of the Clean Air Mercury Rule: EPA-452/R-05-003, 2005. (b) Harris, H. H.; Pickering, I. J.; George, G. N. *Science* **2003**, *301*, 1203.

(4) Nendza, M.; Herbst, T.; Kussatz, C.; Gies, A. *Chemosphere* **1997**, *35*, 1875.

(5) (a) Lovley, D. R.; Coatest, J. D. *Curr. Opin. Biotechnol.* **1997**, *8*, 265. (b) Lovley, D. R. *J. Ind. Microbiol.* **1995**, *14*, 85. (c) Wang, Y-T; Shen, H. *J. Ind. Microbiol.* **1995**, *14*, 159.

(6) Bencheikh-Latmani, R.; Obraztsova, A.; Mackey, M. R.; Ellisman, M. H.; Tebo, B. M. *Environ. Sci. Technol.* **2007**, *41*, 214.

(7) Pagano, G.; Manini, P.; Bagchi, D. *Environ. Health Perspect.* **2003**, *111*, 1699.

(8) Vincent, J. B. *Nutr. Rev.* **2000**, *58*, 67.

(9) (a) Zamani, H. A.; Rajabzadeh, G.; Masrornia, M.; Dejbord, A.; Ganjali, M. R.; Seifi, N. *Desalination* **2009**, *249*, 560. (b) Sanchez-Moreno, R. A.; Gismera, M. J.; Sevilla, M. T.; Procopio, J. R. *Anal. Bioanal. Chem.* **2010**, *397*, 331. (c) Bergamini, M. F.; dos Santos, D. P.; Zanoni, M. V. B. *Sens. Actuators, B* **2007**, *123*, 902. (d) Caballero, A.; Martínez, R.; Lioveras, V.; Ratera, I.; Vidal-Gancedo, J.; Wurst, A.; Tarraga, A.; Molina, P.; Veciana, J. *J. Am. Chem. Soc.* **2005**, *127*, 15666. (e) Zhu, Z.; Su, Y.; Li, J.; Li, D.; Zhang, J.; Song, S.; Zhao, Y.; Li, G.; Fan, C. *Anal. Chem.* **2009**, *81*, 7660.

(10) (a) Suresh, M.; Mandal, A. K.; Saha, S.; Suresh, E.; Mandoli, A.; Di Liddo, R.; Parnigotto, P. P.; Das, A. *Org. Lett.* **2010**, *12*, 5406. (b) Suresh, M.; Shrivastav, A.; Mishra, S.; Suresh, E.; Das, A. *Org. Lett.* **2008**, *10*, 3013. (c) Suresh, M.; Mishra, S. K.; Mishra, S.; Das, A.

Chem. Commun. **2009**, 2496. (d) Wang, C.; Wong, K. M.-C. *Inorg. Chem.* **2011**, *50*, 5333. (e) Wu, Y.; Jing, H.; Dong, Z.; Zhao, Q.; Wu, H.; Li, F. *Inorg. Chem.* **2011**, *50*, 7412. (f) Liu, Y.; Li, M.; Zhao, Q.; Wu, H.; Huang, K.; Li, F. *Inorg. Chem.* **2011**, *50*, 5969. (g) Liu, Q.; Peng, J.; Sun, L.; Li, F. *ACS Nano* **2011**, *5*, 8040. (h) Huang, K.; Yang, H.; Zhou, Z.; Yu, M.; Li, F.; Gao, X.; Yi, T.; Huang, C. *Org. Lett.* **2008**, *10*, 2557. (i) Lim, C. S.; Kang, D. W.; Tian, Y. S.; Han, J. H.; Hwang, H. L.; Cho, B. R. *Chem. Commun.* **2010**, 2388. (j) Ko, S.-K.; Yang, Y.-K.; Tae, J.; Shin, I. *J. Am. Chem. Soc.* **2006**, *128*, 14150. (k) Liu, Z.; Zhang, C.; Li, Y.; Wu, Z.; Qian, F.; Yang, X.; He, W.; Gao, X.; Guo, Z. *Org. Lett.* **2009**, *11*, 795. (l) Qian, F.; Zhang, C.; Zhang, Y.; He, W.; Gao, X.; Hu, P.; Guo, Z. *J. Am. Chem. Soc.* **2009**, *131*, 1460. (m) Yang, H.; Zhou, Z.; Huang, K.; Yu, M.; Li, F.; Yi, T.; Huang, C. *Org. Lett.* **2007**, *9*, 4729.

(11) Rurack, K. *Spectrochim Acta, Part A* **2001**, *57*, 2161.

(12) (a) Förster, T. *Ann. Phys.* **1948**, *2*, 55. (b) Förster, T. *Z. Naturforsch. A: Phys. Sci.* **1949**, *4*, 321. (c) Wieb van der Meer, B.; Coker, G., III; Simon Chen, S.-Y. *Resonance Energy Transfer, Theory and Data*; VCH: Weinheim, Germany, 1994.

(13) (a) Ma, C.; Zeng, F.; Huang, L.; Wu, S. *J. Phys. Chem. B* **2011**, *115*, 874. (b) White, B. R.; Liljestrand, H. M.; Holcombe, J. A. *Analyst* **2008**, *133*, 65. (c) Fang, G.; Xu, M.; Zeng, F.; Wu, S. *Langmuir* **2010**, *26*, 17764. (d) Lee, Y. H.; Lee, M. H.; Zhang, J. F.; Kim, J. S. *J. Org. Chem.* **2010**, *75*, 7159. (e) Xu, M.; Wu, S.; Zeng, F.; Yu, C. *Langmuir* **2010**, *26*, 4529.

(14) (a) Suresh, M.; Mishra, S.; Mishra, S. K.; Suresh, E.; Mandal, A. K.; Shrivastav, A.; Das, A. *Org. Lett.* **2009**, *11*, 2740. (b) Yu, H.; Xiao, Y.; Guo, H.; Qian, X. *Chem.—Eur. J.* **2011**, *17*, 3179. (c) Kumar, M.; Kumar, N.; Bhalla, V.; Singh, H.; Sharma, P. R.; Kaur, T. *Org. Lett.* **2011**, *13*, 1422. (d) He, G.; Zhang, X.; He, C.; Zhao, X.; Duan, C. *Tetrahedron* **2010**, *66*, 9762. (e) Zhang, X.; Xiao, Y.; Qian, X. *Angew. Chem., Int. Ed.* **2008**, *120*, 8145. (f) Zhou, Z.; Yu, M.; Yang, H.; Huang, K.; Li, F.; Yi, T.; Huang, C. *Chem. Commun.* **2008**, 3387.

(15) Nunez, C.; Bastida, R.; Macias, A.; Bertolo, E.; Fernandes, L.; Capelo, J. L.; Lodeiro, C. *Tetrahedron* **2009**, *6531*, 6179.

(16) Resendiz, M. J. E.; Noveron, J. C.; Disteldorf, H.; Fischer, S.; Stang, P. J. *Org. Lett.* **2004**, *6*, 651.

(17) Dujols, V.; Ford, F.; Czarnik, A. W. *J. Am. Chem. Soc.* **1997**, *119*, 7386.

(18) Singh, J.; Carlisle, D. L.; Pritchard, D. E.; Patierno, S. R. *Oncol. Rep.* **1998**, *5*, 1307.

(19) VanWert, A. L.; Gionfriddo, M. R.; Sweet, D. H. *Biopharm. Drug Dispos.* **2010**, *31*, 1.

(20) Sumalekshmy, S.; Fahrni, C. J. *Chem. Mater.* **2011**, *23*, 483.

(21) Valeur, B.; Pouget, J.; Bouson, J. *J. Phys. Chem.* **1992**, *96*, 6545.

(22) (a) Becke, A. D. *J. Chem. Phys.* **1993**, *98*, 5648. (b) Lee, C.; Yang, W.; Parr, R. G. *Phys. Rev. B* **1988**, *37*, 785.

(23) Hehre, W. J.; Radom, L.; Schleyer, P. v. R.; Pople, J. A. *Ab initio Molecular Orbital Theory*; Wiley: New York, 1988.

(24) Frisch, M. J.; Trucks, G. W.; Schlegel, H. B.; Scuseria, G. E.; Robb, M. A.; Cheeseman, J. R.; Scalmani, G.; Barone, V.; Mennucci, B.; Petersson, G. A.; Nakatsuji, H.; Caricato, M.; Li, X.; Hratchian, H. P.; Izmaylov, A. F.; Bloino, J.; Zheng, G.; Sonnenberg, J. L.; Hada, M.; Ehara, M.; Toyota, K.; Fukuda, R.; Hasegawa, J.; Ishida, M.; Nakajima, T.; Honda, Y.; Kitao, O.; Nakai, H.; Vreven, T.; Montgomery Jr., J. A.; Peralta, J. E.; Ogliaro, F.; Bearpark, M.; Heyd, J. J.; Brothers, E.; Kudin, K. N.; Staroverov, V. N.; Keith, T.; Kobayashi, R.; Normand, J.; Raghavachari, K.; Rendell, A.; Burant, J. C.; Iyengar, S. S.; Tomasi, J.; Cossi, M.; Rega, N.; Millam, J. M.; Klene, M.; Knox, J. E.; Cross, J. B.; Bakken, V.; Adamo, C.; Jaramillo, J.; Gomperts, R.; Stratmann, R. E.; Yazyev, O.; Austin, A. J.; Cammi, R.; Pomelli, C.; Ochterski, J. W.; Martin, R. L.; Morokuma, K.; Zakrzewski, V. G.; Voth, G. A.; Salvador, P.; Dannenberg, J. J.; Dapprich, S.; Daniels, A. D.; Farkas, O.; Foresman, J. B.; Ortiz, J. V.; Cioslowski, J.; Fox, D. J. *Gaussian 09*, Revision B.01; Gaussian, Inc: Wallingford, CT, 2010.

(25) (a) Mercury Update: Impact of Fish Advisories. EPA Fact Sheet EPA-823-F-01-011; EPA, Office of Water: Washington, DC, 2001. (b) U.S. EPA, Integrated Risk Information System (IRIS) on Chromium III. National Center for Environmental Assessment, Office of Research and Development: Washington, DC, 1999.

(26) Lee, M. H.; Wu, J.-S.; Lee, J. W.; Jung, J. H.; Kim, J. S. *Org. Lett.* **2007**, *9*, 2501.

(27) Jiang, G. Y.; Wang, S.; Yuan, W. F.; Jiang, L.; Song, Y. L.; Tian, H.; Zhu, D. B. *Chem. Matter* **2006**, *18*, 235.